Title	Visualizing orbital angular momentum of plasmonic vortices
Author(s)	Shen, Z.; Hu, Zongjiang; Yuan, Guanghui; Min, C. J.; Fang, H.; Yuan, Xiaocong
Citation	Shen, Z., Hu, Z., Yuan, G. H., Min, C. J., Fang, H., & Yuan, X.-C. (2012). Visualizing orbital angular momentum of plasmonic vortices. Optics Letters, 37(22), 4627-4629.
Date	2012
URL	http://hdl.handle.net/10220/10929
Rights	© 2012 Optical Society of America. This paper was published in Optics Letters and is made available as an electronic reprint (preprint) with permission of Optical Society of America. The paper can be found at the following official DOI: [http://dx.doi.org/10.1364/OL.37.004627]. One print or electronic copy may be made for personal use only. Systematic or multiple reproduction, distribution to multiple locations via electronic or other means, duplication of any material in this paper for a fee or for commercial purposes, or modification of the content of the paper is prohibited and is subject to penalties under law.

Visualizing orbital angular momentum of plasmonic vortices

Z. Shen,[1,†] Z. J. Hu,[2,†] G. H. Yuan,[3,4] C. J. Min,[1] H. Fang,[1] and X.-C. Yuan[1,5]

[1]*Institute of Modern Optics, Key Laboratory of Optical Information Science & Technology, Ministry of Education of China, Nankai University, Tianjin 300071, China*

[2]*CAS Key Laboratory of Standardization and Measurement for Nanotechnology, National Center for Nanoscience and Technology, Beijing 100190, China*

[3]*School of Electrical & Electronic Engineering, Nanyang Technological University, Nanyang Avenue, Singapore 639798, Singapore*

[4]*e-mail: ghyuan@ntu.edu.sg*

[5]*e-mail: xcyuan@nankai.edu.cn*

Received July 9, 2012; revised September 24, 2012; accepted September 28, 2012; posted October 1, 2012 (Doc. ID 172228); published November 7, 2012

Plasmonic vortices (PVs) are generated by focusing a radially polarized optical vortex (OV) beam onto a metal surface. The intensity distribution of the PV is registered with a near-field scanning optical microscopy and agrees well with a theoretical prediction as well as numerical calculation. Beside the dark central spot, the numerical calculation also shows an azimuthal Poynting vector belonging to the PV, implying that the orbital angular momentum (OAM) was transferred from the radially polarized OV. To directly verify the OAM, plasmonic trapping experiments with gold micrometer particles are performed and the particle rotation is visualized. Further experiments by varying the topological charge of radially polarized OVs show the corresponding changes in rotation in terms of speed and radius.

OCIS codes: 240.6680, 050.4865, 180.4243.

Orbital angular momentum (OAM) of optical vortices (OVs) has widely been studied in the optics regime in areas such as optical manipulation, microscopic image processing, and information communications [1–3]. Recently, the counterpart whirlpools of OV in terms of evanescent surface plasmon polaritons (SPPs), which are referred to as plasmonic vortices (PVs), have been reported, and their implied OAM has also been addressed in the framework of intensity distribution analysis [4–7], showing potential applications in manipulation of matter such as atoms [8,9]. It was found that the extrinsic OAM of the SPP can be produced not only by forming the geometric phase retardation with nanogrooves but also by coupling the intrinsic spin angular momentum of the incident radiation in coaxial nanoapertures [10,11]. However, the physics properties of PVs' OAM related to being capable to trap and rotate particles, with an analogy to OV OAM, are still waiting to be explored.

In this Letter, we realize a dynamic generation of PVs by focusing a radially polarized OV beam onto a metal surface (Fig. 1). Compared to the generation by surface-relief spiral grooves or plasmonic vortex lens [5–7], our method benefits from the structureless excitation of the SPP with a dynamic control, therefore reducing the requirements for center alignment and fabrication of complex structures in the nanometer scale. Previously, we studied the SPP generation from a linearly polarized OV [12,13], where standing waves with central phase singularity are formed, but the OAM of the incident OV cannot be retained in this case due to the central asymmetric polarization. Changing to the current radially polarized OV enables the OAM transformation to SPP while still keeping the phase singularity. Subsequently, we directly verify the existence of PVs' OAM by plasmonic trapping experiments with gold micrometer particles. With the particles distributed on the metal surface and interacting with PVs, it is natural to anticipate the visualization of particle rotation. Although optical OAM manipulations by conventional OV have widely been reported in terms of angular momentum conversion between the light beam and the trapped particles [14,15], plasmonic OAM manipulation, to the best of our knowledge, has not been implemented thus far. It represents a great challenge because of its near-field nature.

As for our experimental setup, shown in Fig. 1, the radially polarized OV is achieved after the circularly polarized beam with a wavelength of 633 nm (He–Ne laser) sequentially passes through a spiral phase plate encoded with a topological charge l, an azimuthal-type polarization analyzer, and a polarization rotator (PR) [16]. The PR consists of two half-wave plates and can switch the polarization state of the beam between azimuthal and radial polarization by turning one of the two half-wave plates by 45°. When the handedness of the circular polarization beam is in the same (or opposite) direction as the phase increment of the spiral phase plate, the radially polarized OV with a topological charge of $l+1$ (or $l-1$) is produced. Finally, the radially polarized OV beam is then relayed via a telescope into the rear aperture of an oil-immersion objective lens (Olympus 100×, NA 1.49) and focused onto a 50 nm thick Au film (with $\varepsilon_2 = -9.514 + 1.218i$ at the wavelength of 633 nm) deposited on a standard cover glass ($n = 1.515$, thickness 100 μm) to excite SPPs on the top surface of the metallic layer, and the surface plasmon resonance (SPR) angle is about 44.5°. The excited SPP can be scanned with near-field scanning optical microscopy (NSOM) (NT-MDT, NTEGRA Solaris) using an aluminum-coated fiber tip with a 100 nm diameter aperture operating in collection mode 60 nm above the Au film surface. The attainable resolution is below 100 nm.

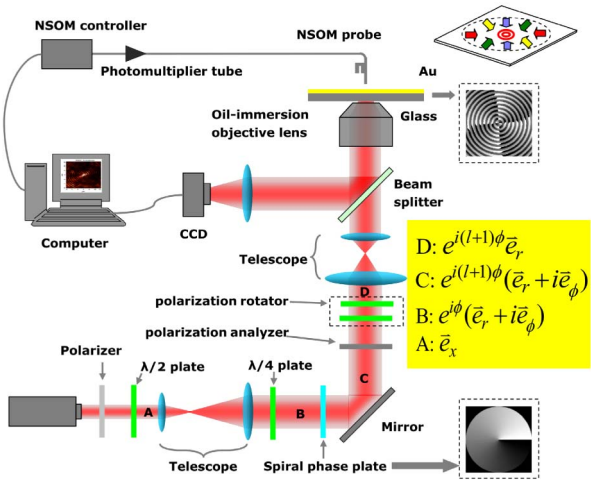

Fig. 1. (Color online) Schematic diagram of experimental setup. The polarization states corresponding to the positions denoted by capital letters A, B, C, and D in the optical path are given in the yellow square. The phase distribution of a spiral phase plate with topological charge $l = 1$ is given in the lower right dashed box as an example. The phase distribution of the E_z component of the PV of $l = 2$ is given at the right side of the Au film. The red, green, blue, and yellow arrows in the upper right inset show the corresponding E_z component with relative phase differences of 0, $\pi/2$, π, and $3\pi/2$, respectively.

Figure 2 shows the intensity distribution of generated PV with $l = 2$, which is sensitive to the in-plane electric field component. As can be clearly seen from the NSOM image in Fig. 2(a), an SPP standing-wave interference pattern is formed on the metal surface. Figure 2(b) gives a better display of the phase singularity at the image center, where the period of the interference can also be extracted as 298 ± 2 nm. This value agrees well with the theoretical prediction, as will be discussed next.

First note that the electric field of tightly focused, radially polarized OV has radial (E_r), azimuthal (E_φ), and longitudinal (E_z) components according to the Richard–Wolf vectorial diffraction theory [17,18], where E_z is prominently enhanced in comparison with the two transverse components after passing the Au film. Therefore E_z will play a dominant role in characterizing the electric field distribution on the metal surface. Similar to that described in [12,13], the SPP will be excited at a typical SPR angle and act as a secondary circular source propagating inward to the center when the Au film is located before the focal plane of the objective lens. The longitudinal plasmonic field in the central region hence can be expressed mathematically as

$$E_{1z}(r,\varphi,z) = \int_0^{2\pi} E_{1z} e^{il\theta} e^{-k_z z} e^{-ik_{sp}\vec{e}_{r'}\cdot(\vec{r}-\vec{R}_0)} d\theta$$
$$= E_{1z} e^{-k_z z} e^{ik_{sp}R_0} e^{il\varphi} J_l(k_{sp} r), \quad (1)$$

where E_{1z} represents the initial amplitude of the above-mentioned circular SPP source along the circumference with excitation radius R_0, (r, φ, z) is the observation point in cylindrical coordinates, and k_{sp} and k_z are the transverse and longitudinal wave vectors, respectively. Only the symmetric mode is considered here because the asymmetric mode with a refractive index ~1.778 cannot be excited in this configuration. Equation (1) shows that the plasmonic field is dominated by the Bessel function $J_l(k_{sp}r)$ and also owns a spiral phase factor $\exp(il\varphi)$, which agrees with the well-known results in [7] but has been derived under a different excitation mechanism.

A further theoretical investigation is conducted by three-dimensional finite-difference time-domain numerical method with the FullWAVE module of the commercial RSOFT software, where the size of the discretization unit cells is 25 nm in the x and y directions and 5 nm in the z direction, perfectly matched layer boundary conditions are set for all three directions, and the data points are taken from the x-y plane 60 nm above the Au film within the longitudinal decay length of the SPP field (284 nm). As shown in Fig. 3(a), $E_{1z}(r, \varphi, z)$ has a primary peak ring accompanied by a series of concentric outer rings with gradually diminished amplitude. The period of the SPP pattern is found to be 298 nm, which proves our experimental results in Fig. 2. We also obtained the time-averaged Poynting vectors in the same observation plane, where an azimuthal energy flow can be clearly seen. According to the vector description for PV [7], the major component of the Poynting vector should be the azimuthal component and the longitudinal component should be zero because the evanescent field does not carry any energy flow along the decaying direction. The azimuthal energy-flow pattern shown in Fig. 3(b) indicates that an OAM has been established inside the PV.

To directly verify that the incident OV confers a well-defined OAM to the PV, we performed a plasmonic trapping experiment with gold micrometer particles. The circumferential rotation of the particle near the PV focal region has indeed been observed, as shown

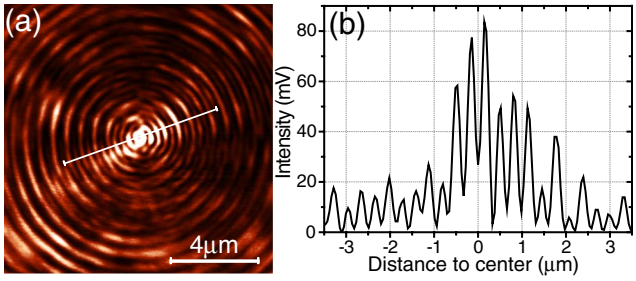

Fig. 2. (Color online) (a) Experimental NSOM image of the SPP distribution excited by the highly focused, radially polarized OV at 633 nm incident wavelength. (b) Intensity distribution along the white line in (a).

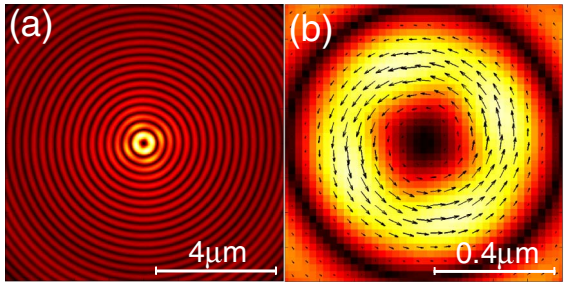

Fig. 3. (Color online) (a) Amplitude distributions of the E_z component with topological charge $l = 2$. (b) Time-averaged Poynting vector near the primary ring of the PV.

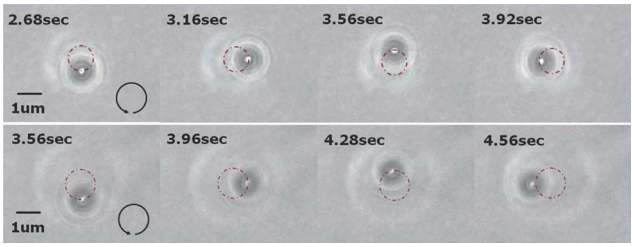

Fig. 4. (Color online) Successive frames of video recordings that show the rotation of a single gold particle trapped by PVs of $l = 2$ (top row, Media 1) and $l = 5$ (bottom row, Media 2). The circular arrow denotes the rotation direction, and the dashed circles show the particle's orbital trajectory.

in Fig. 4. Gold particles were chosen due to their strong absorption and scattering in order to boost the transfer of the OAM from the PV to the particles. In the experiment, the gold particles ($0.8 \sim 1.5$ μm, ALFA AESAR) were diffused in water and then injected into an in-house-fabricated chamber on the gold film. This experimental system used has undergone some changes from that shown in Fig. 1: a different working wavelength of 1064 nm (Nd:YAG laser) is employed considering its high optical power, the NSOM tip is replaced with an optical fiber illuminator (Thorlabs OSL 1-EC) to enable imaging the moving particles with the CCD camera (Point Grey Chameleon CMLN-13S2M), the beam splitter is replaced with a dichroic mirror (highly transmissive at 1064 nm and highly reflective for visible light), and a low-pass filter is positioned in front of the CCD camera to filter out the 1064 nm stray light. The SPR angle was shifted to 63.4° but was still within the range of the objective lens. To make a quantitative comparison, the incident power measured by a power meter before the beam entered the objective lens was adjusted to 160 mW.

During the experiment, it is interested to observe that when the radially polarized OV was switched to the azimuthally polarized OV, the rotating particle stopped immediately (begin with 4 s in Media 1 and 5 s in Media 2), and when the radially polarized OV was turned back, the paused rotation recovered. The switch between these two polarization states is realized via PR (Fig. 1). It unambiguously verifies the PV OAM because for azimuthally polarized OV no SPP excitation is expected and there is no force exerted on the particle.

As shown in Fig. 4, it is found that when the topological charge of the radially polarized OV changes from $l = 2$ to $l = 5$, the particle rotation changes accordingly where the radius enlarges and the speed increases. The rotation radius under $l = 2$ (Media 1) and $l = 5$ (Media 2) are obtained respectively as 0.44 and 0.77 μm, and the rotation speed under $l = 2$ and $l = 5$ respectively as 2.0 and 2.3 μm/s. Therefore, the product of the radius and the speed under $l = 5$ appears to be 2.01 times that under $l = 2$. Following the theory developed by Barnett and Allen [19,20], this ratio should be 5/2. The difference could be caused by the variable coupling efficiency from radially polarized OV to PV under different l, owing to the slightly different incident optical energy in the specific angle exciting SPPs before focusing and different optical power exerting on the particles, and also by the possible slight difference in particle mass as two different particles are trapped.

In summary, we have experimentally generated a PV in an all-optical and dynamic manner by tightly focusing radially polarized OV onto a planar metal surface, and we directly visualized the OAM of the PV by rotating gold particles circumferentially around the PV center. Under tight focusing, the incident radially polarized OV can transfer its azimuthal phase as well as OAM to the PV, leading to the confinement and manipulation of metal particles within the plasmonic evanescent field region. Its prospective applications with metal particles in optical tweezers, surface-enhanced Raman spectroscopy, and florescent microscopic imaging with super resolution are highly expected.

This work was partially supported by the National Natural Science Foundation of China under grant nos. 10974101, 61036013, and 61138003, the Ministry of Science and Technology of China under grant no. 2009DFA52300 for China-Singapore collaborations, and the National Research Foundation of Singapore under grant no. NRF-G-CRP 2007-01. X.-C. Y acknowledges the support given by Tianjin Municipal Science and Technology Commission under grant no. 11JCZDJC15200.

†Authors contributed equally to this Letter.

References

1. M. Padgett and R. Bowman, Nat. Photonics **5**, 343 (2011).
2. L. Allen, M. W. Beijersbergen, R. J. C. Spreeuw, and J. P. Woerdman, Phys. Rev. A **45**, 8185 (1992).
3. G. Molina-Terriza, J. P. Torres, and L. Torner, Nat. Phys. **3**, 305 (2007).
4. A. T. O'Neil, I. MacVicar, L. Allen, and M. J. Padgett, Phys. Rev. Lett. **88**, 053601 (2002).
5. T. Ohno and S. Miyanishi, Opt. Express **14**, 6285 (2006).
6. S. Y. Yang, W. B. Chen, R. L. Nelson, and Q. W. Zhan, Opt. Lett. **34**, 3047 (2009).
7. H. Kim, J. Park, S. W. Cho, S. Y. Lee, M. Kang, and B. Lee, Nano Lett. **10**, 529 (2010).
8. D. L. Andrews, M. Babiker, V. E. Lembessis, and S. Al-Awfi, Phys. Stat. Sol. Rapid Res. Lett. **4**, 241 (2010).
9. V. E. Lembessis, S. Al-Awfi, M. Babiker, and D. L. Andrews, J. Opt. **13**, 064002 (2011).
10. Y. Gorodetski, N. Shitrit, I. Bretner, V. Kleiner, and E. Hasman, Nano Lett. **9**, 3016 (2009).
11. Y. Gorodetski, A. Niv, V. Kleiner, and E. Hasman, Phys. Rev. Lett. **101**, 043903 (2008).
12. P. S. Tan, X.-C. Yuan, G. H. Yuan, and Q. Wang, Appl. Phys. Lett. **97**, 241109 (2010).
13. P. S. Tan, G. H. Yuan, Q. Wang, N. Zhang, D. H. Zhang, and X.-C. Yuan, Opt. Lett. **36**, 3287 (2011).
14. H. He, M. E. J. Friese, N. R. Heckenberg, and H. Rubinsztein-Dunlop, Phys. Rev. Lett. **75**, 826 (1995).
15. Y. Q. Zhao, J. S. Edgar, G. D. M. Jeffries, D. McGloin, and D. T. Chiu, Phys. Rev. Lett. **99**, 073901 (2007).
16. K. J. Moh, X.-C. Yuan, J. Bu, R. E. Burge, and Bruce Z. Gao, Appl. Opt. **46**, 7544 (2007).
17. B. Richard and E. Wolf, Proc. Roy. Soc. A **253**, 358 (1959).
18. K. S. Youngworth and T. G. Brown, Opt. Express **7**, 77 (2000).
19. S. M. Barnett and L. Allen, Opt. Commun. **110**, 670 (1994).
20. M. E. J. Friese, J. Enger, H. Rubinsztein-Dunlop, and N. R. Heckenberg, Phys. Rev. A **54**, 1593 (1996).